Full Waveform Seismic Tomography for geophysical velocity model in South Island region, New Zealand using broadband data and Adjoint-Wavefield method

Trung Dung Nguyen [1], Robin Lee [1], Brendon Bradley [1], Robert Graves[2]

[1] University of Canterbury, New Zealand, [2] USGS, Pasadena

andrei.nguyen@Canterbury.ac.nz

1. Introduction

In this poster we apply Full Waveform Tomography (FWT) based on the Adjoint-Wavefield (AW) method to iteratively invert a 3-D geophysical velocity model for the South Island region, New Zealand (Eberhart-Phillips, 2010). The seismic wave fields were generated using numerical solution of the 3-D visco- elastodynamic equations, and through the AW method, gradients of model parameters (compressional and shear wave velocity) were computed by implementing the cross-adjoint of forward and backward wavefields. The misfit measure is a frequency-dependent multi-taper travel-time difference using a period range 10 - 40 s. The main computational cost relates to the computation of the gradient of misfit function for each event (event kernel). We used L-BFGS/ parabola fitting algorithms to obtain a model update. To verify the method's performance, the synthetic study using 16 events and 25 stations equally distributed shows a good convergence of the inverted velocity models to the given true models (checker board). For real data analysis, simulation-to-observation misfit measurements based on 13 sources at 10 seismic broad band stations in the Northern part of the South Island were used into the first stage of our inversion, and including more events at the later stage. Each stage was used for up to 10 iterations or no significant decrement of the misfit.

After each FWT inversion run, the simulated seismograms computed using our final velocity model show the misfit error has been significantly reduced. The histograms of the relative waveform misfit and travel time difference between observed and simulated data generated by the initial and inverted models for a fixed set of windows also indicate the improvement of the simulated waveform comparing to the observed seismograms at frequencies from 0.025 - 0.1 Hz. A ground motion validation test was also performed which shows the improvement of the ground motion prediction.

2. Waveform segmentation using Pyflex and adjoint source construction/ misfit calculation using Pyadjoint

To set up the full waveform tomography problem, we solve the forward wave propagation problem using the Stress-Velocity formulation of 3D visco-elastic wave equations (Graves, 1996) in the software emod3d. We then define a misfit function between the observed data recorded at seismic stations for different events and the simulated data from our forward simulation using an inverted source and a given velocity model. From the defined misfit function, we construct the Frechet derivatives based on seismic data inversion theory. We then consider the adjoint-wavefield method, which back-propagates the data to attract information of the medium structure. To construct the adjoint source for backward simulation, we implemented the multi-taper method (Tape, 2009). We utilized Pyflex - an automated time-window selection algorithm for seismic tomography (Maggi et al., 2009; Krischer et al., 2015b) and Pyadjoint for measurement of frequency-dependent phase differences estimated with multitaper approach (Krischer et al., 2015a). For adjoint simulation, the adjoint sources calculated for each events were injected simultaneously at all station locations and for all 3 components.

The observed seismograms were achieved from FDSN protocol provided by GeoNet and resampled to the simulation time step) with recorded time of 200s. The simulated data were generated using a point source for each event with the CMT solution provided by GeoNet (Ristau, 2008) and a given 3-D velocity model. Pyflex package has been utilized for segmentation of the observed and synthetic seismograms. The multi-taper approach of misfit calculation and adjoint source construction were performed on windowed sections of the seismograms using the Pyadjoint package. By tuning parameters similar to tomographic scenarios of Southern California (Maggi, 2009; Tape, 2009) as well as New Zealand's scenarios (Chow, 2019) and using synthetic data generated from a 3-D velocity model, we are able to pick up a window specified by the start time and end time, cross-correlation coefficient, travel time difference and the amplitude difference. Figure 1a shows the example of Pyflex segmentation for a pair of observed and simulated data. Figure 1b shows the adjoint source and the misfit calculated using Pyadjoint.

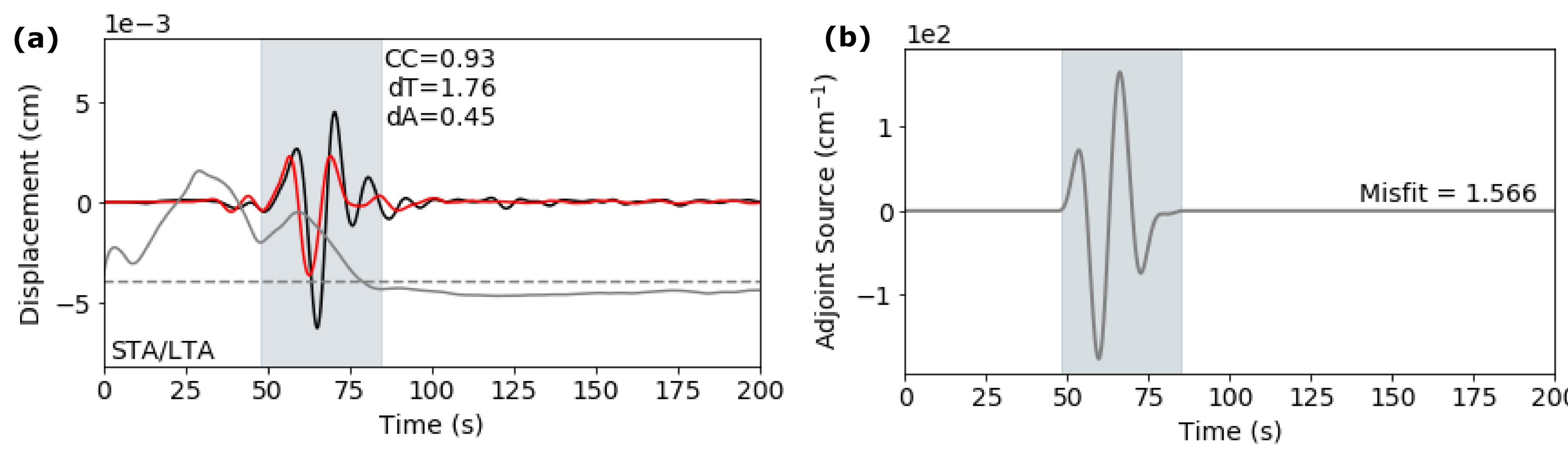

Figure 1: (a) Displacement seismogram (radial component - 090) of the observed data (black) from broadband station KHZ for event 3505099 and the synthetic data (red) generated from the initial model m00 according to the same event and station. Observed seismograms and synthetic seismograms are filtered over the period range 10 to 40 s (0.025 to 0.1 Hz. Gray rectangle presents window picked by Pyflex. (b) Adoint sources (without reversing in time) and misfit calculated by Pyadjoint for the pairs of given windowed seismograms.

3. Automated workflow and computational demand

Simulation domains of 352x352x160 km are derived from a detailed velocity model of a 3-D geophysical velocity model for the South Island region, New Zealand using 4km grid size (Figure 2a). The horizontal view of the initial *Vs* profile at 4km depth includes 13 sources and 10 stations using for the first inversion stage (Figure 2b). For each simulation, the recorded time is 200s and time step is 0.16s. For each event, a forward and a backward (adjoint) simulations are performed to extract strain wavefields for kernel calculation. These strain wavefields store strain components for every single cell in the domain and for every 5 time steps. For total 13 events, the computation was divided to an automated parallel mode in Nesi's supercomputer (Maui). In addition to the kernels calculation, the optimal step length calculation for model updating also requires multiple forward modelling and storage of gradients and models for at least 2 previous iterations for implementation of L-BFGS method. One iteration of the inversion costs approximately 200 core hours and occupies 4 computing nodes at a time.

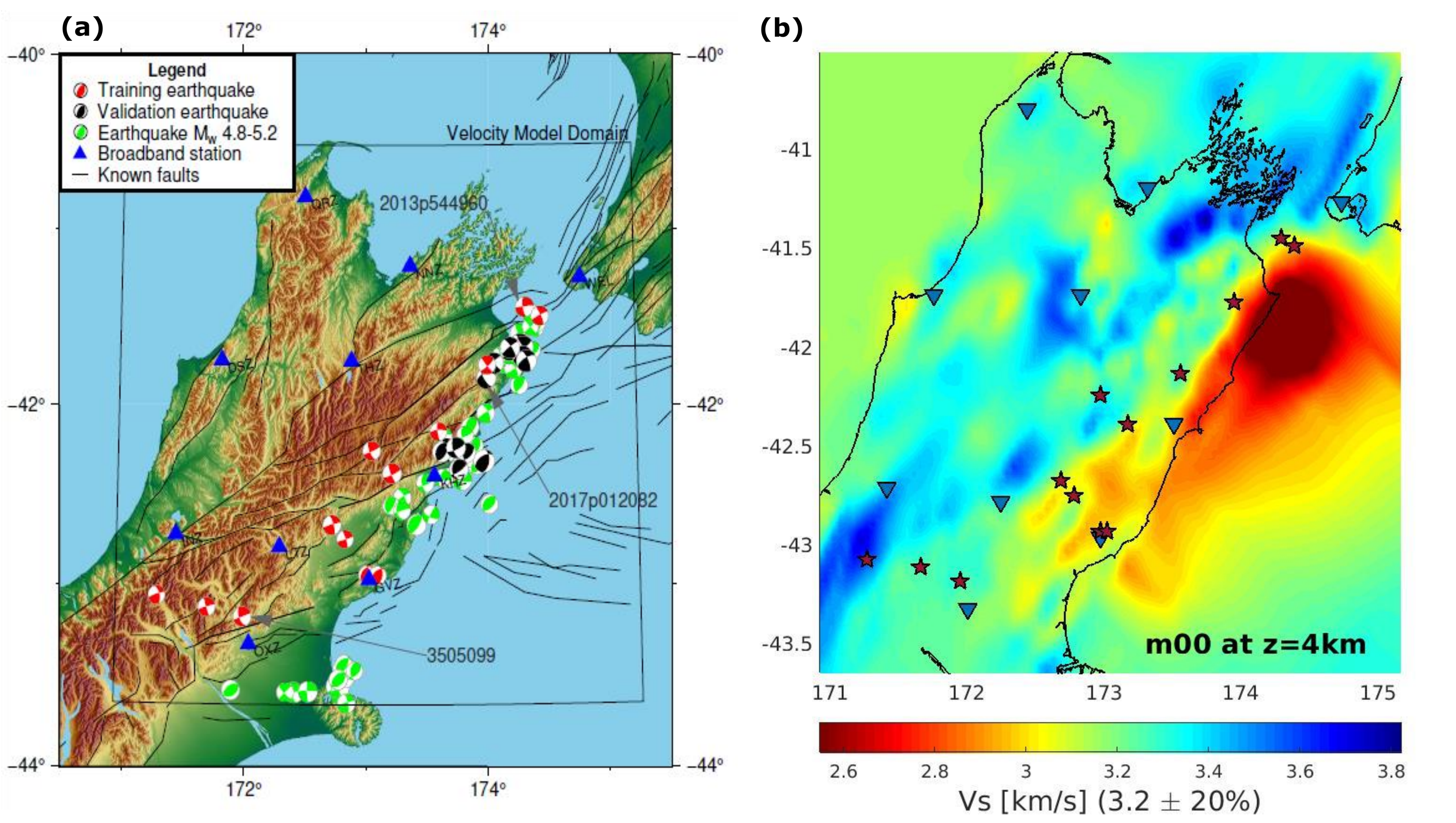

Figure 2: (a) Topography map of the South Island region, New Zealand with event (beach ball)/ station (triangle) locations; (b) Initial 3D velocity model for *Vs* used for inversion.

References

1. Maggi, A., Tape, C., Chen, M., Chao, D., and Tromp, J., 2009. An automated time-window selection algorithm for seismic tomography.Geophysical Journal International178, 257–281.
2. Krischer, L., Fichtner, A., Zukauskaite, S., and Igel, H., 2015a. Large-scale seismic inversion framework.Seismological Research Letters86, 1198–1207.
3. Krischer , et al. 2015b. ObsPy: A bridge for seismology into the scientific Python ecosystem.Computational Science & Discovery8, 014003.
4. Chow, B., Kaneko, Y., Modrak, R., Tape, C., and Townend, J., 2019. A semi-automated adjoint tomography workflow applied to New Zealand's North Island.AGUFM2019, S34A–02.
5. Tape, Carl, et al. "Adjoint tomography of the southern California crust." Science 325.5943 (2009): 988-992.
6. Ristau, John. "Implementation of routine regional moment tensor analysis in New Zealand." Seismological Research Letters 79.3 (2008): 400-415.
7. Graves, Robert W. "Simulating seismic wave propagation in 3D elastic media using staggered-grid finite differences." Bulletin of the Seismological Society of America 86.4 (1996): 1091-1106.
8. Eberhart-Phillips, D., Reyners, M., Bannister, S., Chadwick, M., and Ellis, S., 2010. Establishing a435versatile 3-D seismic velocity model for New Zealand.Seismological Research Letters81, 992–1000.

Acknowledgements

The numerical simulations were performed on Nesi's supercomputer. The work was funded by University of Canterbury and QuakeCore. We thank Donna Eberhart-Phillips for providing the background model NZVM 2010 included in the tomographic inversion and GeoNet for providing the earthquake catalogue and broadband station data used in this study.

4. Checkerboard test

To investigate the accuracy/ efficiency for the wave propagation solution and the inversion algorithm, a checker board test was implemented (Figure 3). The experimental set-up for the checker board test was shown in Figure 4a with an uniform grid of 16 events and 25 station; and the difference between the true and the initial Vs (in log-scale). The sources are the same with depth=8km, strike=90, dip=45, rake=90 and Mw=5.5. Data are filtered from 0.025-0.1Hz.

After 10 iterations, the inverted model has been converging toward the true model. Figure 4b shows the difference between the inverted and the initial Vs (in log-scale) at 12km depth. The frequency-dependent phase differences between observed and synthetic data (misfit-red) decreased from 0.95 to 0.25 after 10 iterations and the number of windows picked increases along with the misfit reduction also presented in Figure 4c.

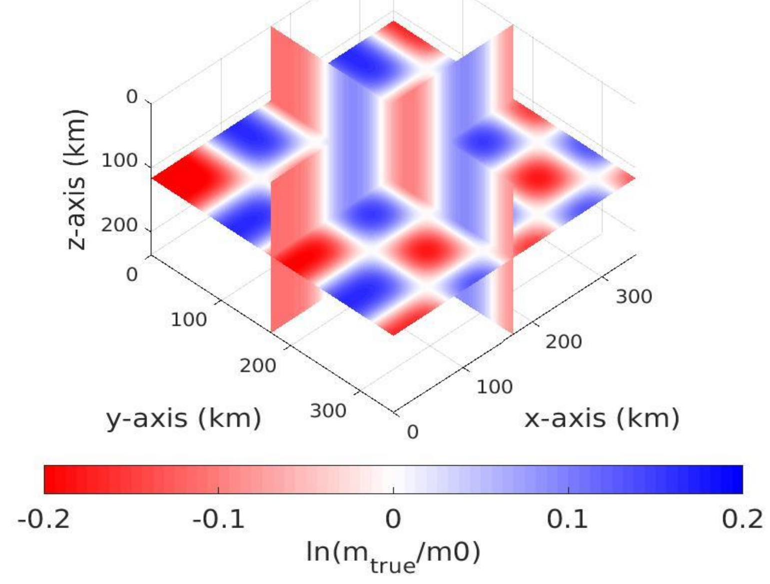

Figure 3: Checker board 3-D view. The minimum and maximum per cent perturbations in the true model (checker board) are ±20 per cents.

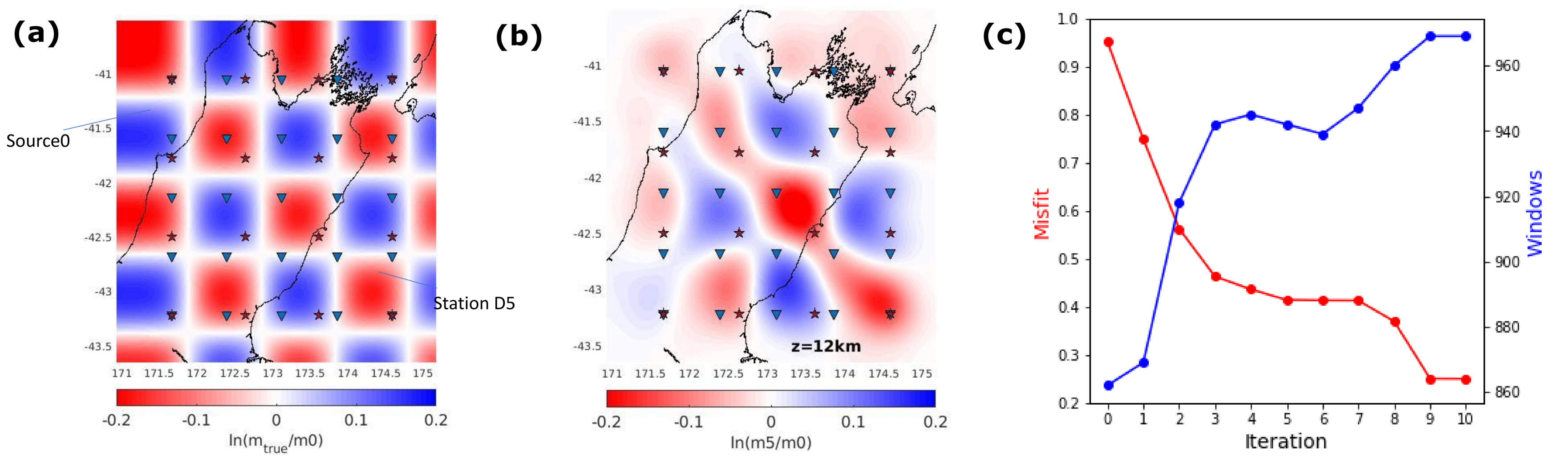

Figure 4: The checker board test: (a) difference between the true and the initial Vs (in log-scale) at any depth, (b) difference between the inverted and the initial Vs (in log-scale) at 12km depth, (c) Misfit (red) and number of windows (blue) along iterations.

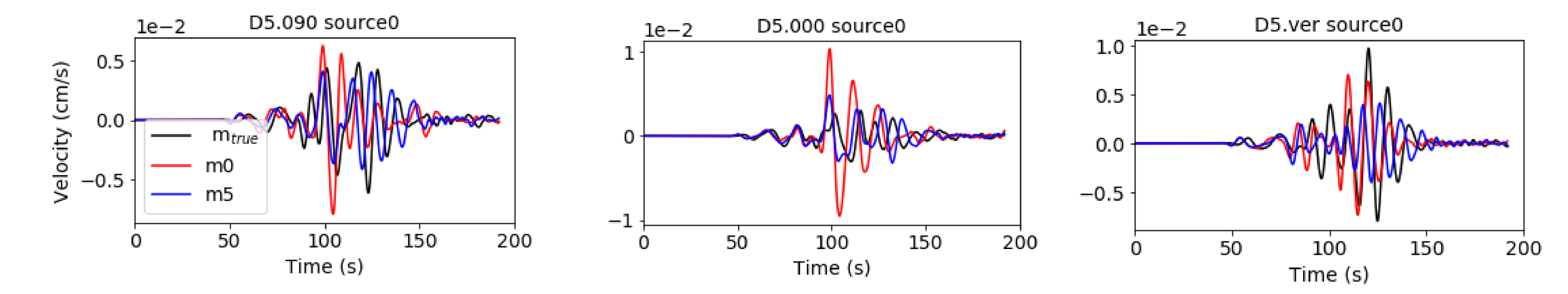

Figure 5: Waveform comparison for 3 components of the velocity seismograms according to source0, station D5. Black (observed), red and blue lines are the synthetic data generated from the true model, initial model (m0) and inverted model (m5) accordingly.

As a result of the velocity model update, there is a good agreement between the observed and estimated data (filtered through a bandwidth of 0.025-0.1 Hz) only after 5 iterations (Figure 5). The good recover of the checker board using the presented FWT technique suggests the applications for inversion of broadband data.

5. Broadband data inversion result

The broadband data from 13 Earthquakes with Mw 4.8-5.2 and hypocenter varying from 4 to 20km depth, recorded by 10 broad band stations in the area were included in this study. This set of earthquake events was chosen based on the consistent of the data quality, the source magnitude and the balance of geometrical distribution (Figure 1a). Another set of larger earthquake Mw 5.2-6.0 was also present as a reference set for accessing the improvement of the velocity model after iterations and additional data for inversion at the later stage. Our inversion included 1170 three-component and only seismograms with normalized correlated coefficient larger than 0.7 and maximum time shift less than 10s are used for inversion. After 10 iterations, the misfit between observed and synthetic data has been reduced significantly (Figure 6d). We present our inverted Vs model after 10 iterations on both absolute value (Figure 6b) and relative change (Figure 6c) comparing to the initial model (Figure 6a) at 12 km depth. The variation of shear wave velocities from depth 4 km to 20 km all over the domain was from 25% decreasing to 17% increasing.

We then compared the relative waveform misfit and travel time shift (Figure 7) for a fixed set of windows picked according to the initial model and 13 events included in the inversion and another set for 14 events not included the inversion. The waveform comparison for the event 2013p544960 and station GVZ at 2 different iterations are shown in Figure 8. Ground motion simulation validation was performed for the inverted model m10 refined to 200m-grid (with maximum resolvable frequency of 0.5Hz) using 1798 ground motions from 76 events (small magnitude) and 176 strong motion and broadband stations which shows slight reduction of the model prediction bias in Fourier amplitude spectra up to 0.5Hz compared to the initial model.

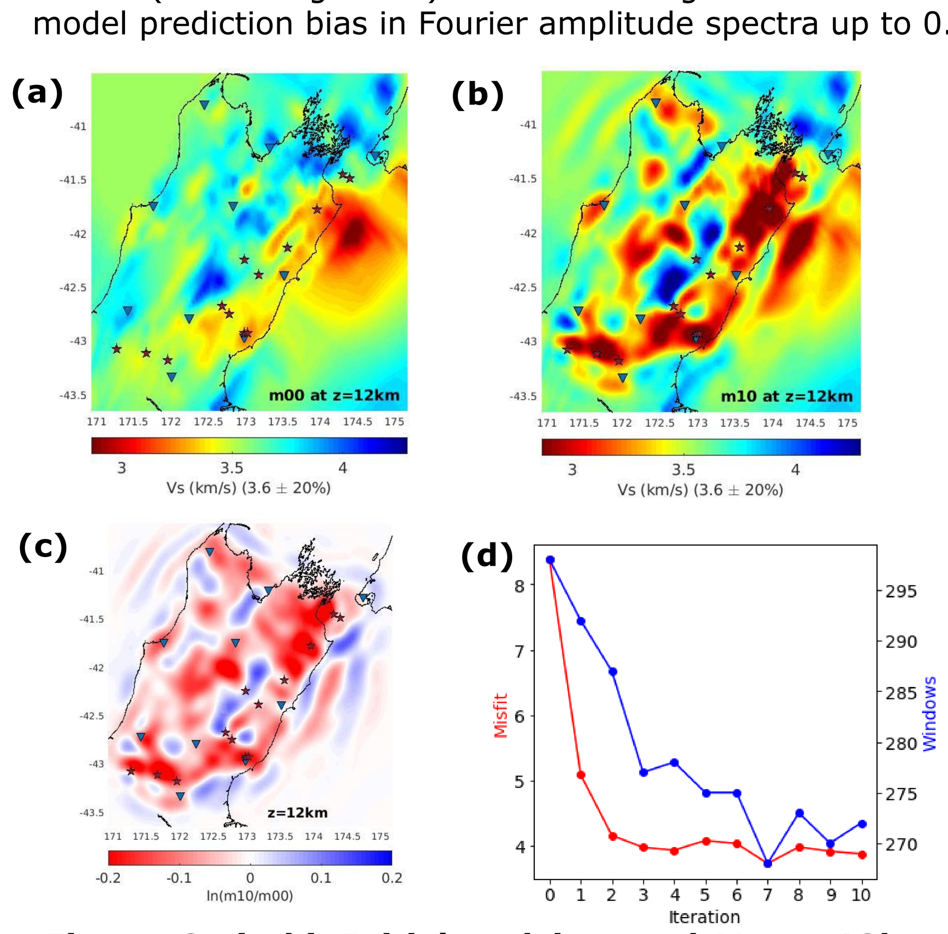

Figure 6: (a-b) Initial and inverted Vs at 12km depth; (c) Model difference (log-scale); (d) Misfit (red) and number of windows (blue) along iterations.

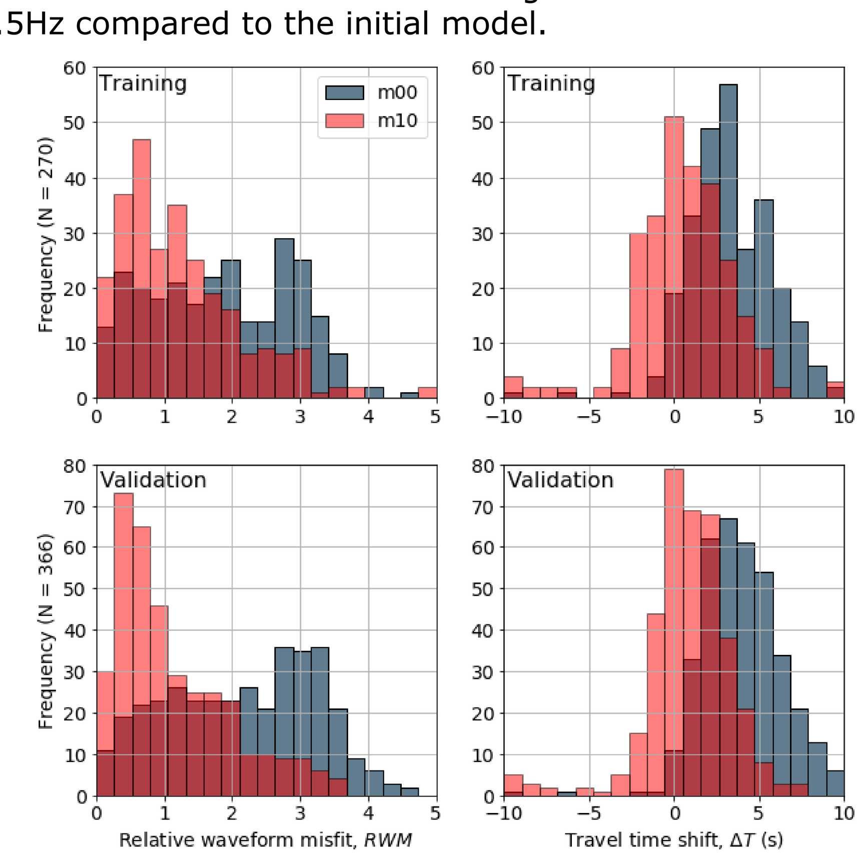

Figure 7: Histograms of relative waveform misfit (left) and travel time shift (right) for initial model (grey) and inverted model (red) according to "Training events" (top) and "Validation events" (bottom).

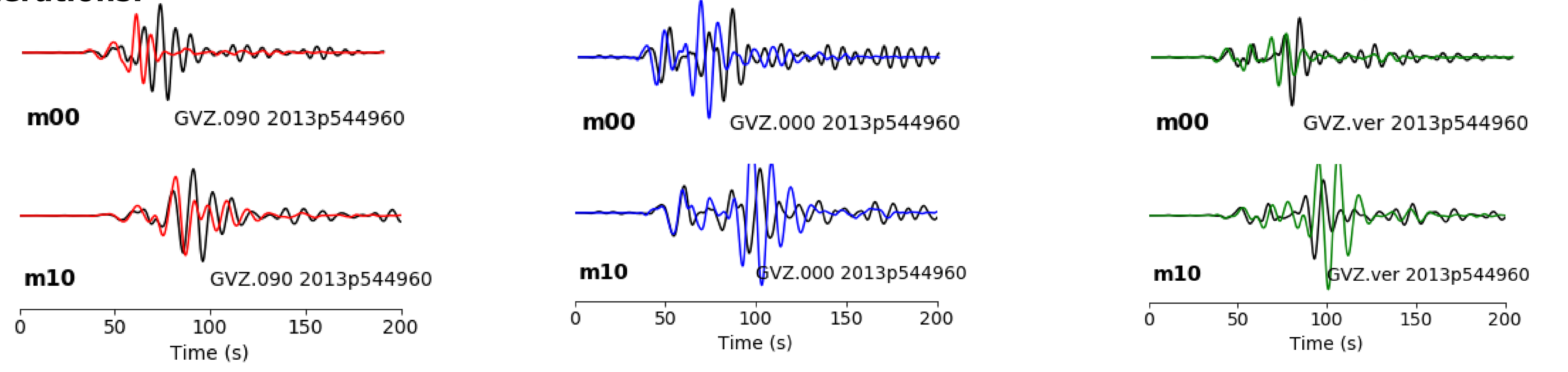

Figure 8: Waveform comparison between the observed data (black) and synthetic data for 2 models m00 (initial) and m10 (inverted) for station GVZ according to event 2013p544960.

6. Future study

Since continuing inversion after iteration 10 using 13 events data does not improve the model significantly, we navigate the inversion further by adding more events (14 reference events). The further development of the method is to refine the inverted model at smaller grid and increase the frequency content of the broadband data together with revising the centroid moment tensor solutions for the sources.